Chinese Chemical Letters 33 (2022) 3049–3052

Contents lists available at ScienceDirect

Chinese Chemical Letters

journal homepage: www.elsevier.com/locate/cclet

Cu-clusters nodes of 2D metal-organic frameworks as a cost-effective noble-metal-free cocatalyst with high atom-utilization efficiency for efficient photocatalytic hydrogen evolution

Guangmei Jiang[a], Xingyan Liu[a,*], Huilong Jian[a], Peng Lu[a], Jinwu Bai[a], Guizhi Zhang[a], Wen Yun[a], Siqi Li[b], Youzhou He[a,*]

[a] Chongqing Key Laboratory of Catalysis and New Environmental Materials, College of Environment and Resources, Chongqing Technology and Business University, Chongqing 400067, China
[b] State Key Joint Laboratory of Environment Simulation and Pollution Control, School of Environment, Tsinghua University, Beijing 100084, China

ARTICLE INFO

Article history:
Received 15 June 2021
Revised 3 August 2021
Accepted 12 September 2021
Available online 17 September 2021

Keywords:
2D nanosheets
Photocatalytic hydrogen production
Cu-clusters nodes
Cu^{II}/Cu^{I}
Cocatalysts

ABSTRACT

Several 2D nanosheets of porphyrin MOFs with various transition-metal clusters as metal nodes were prepared *via* a simple solvothermal method to apply in the photocatalytic hydrogen evolution, in which the hydrogen production rate of the optimal NS-Cu was as high as 15.39 mmol g^{-1} h^{-1}. A series of experimental technologies especially cyclic voltammetry (CV) and Mott-Schottky (M-S) had been adopted to investigate the charge-transfer property of photo-generated electron-hole pairs, it was found that the uniformly dispersed Cu-clusters nodes in the original 2D MOFs played a key role in the electron transfer process, that was, the photo-generated electron transferred from excited state eosin-Y to the Cu-clusters nodes for the efficient hydrogen evolution. The excellent photocatalytic performance could be attributed to the reversible oxidation-–reduction process of Cu^{II}/Cu^{I}, which had excellent electron-receiving and electron-outputting capabilities. Our results provided a novel avenue to adapt the uniformly dispersed metal nodes in the original MOFs as cost-effective noble-metal-free cocatalysts with very high atom-utilization efficiency to improve the photocatalytic hydrogen evolution performance in dye-sensitized system.

With the rapid development of human economy and civilization, the urgent demand for energy consumption especially fossil fuels gradually increases, accompanied by more and more serious environmental problems [1–5]. In comparison with fossil fuels, hydrogen has the advantage of high combustion value that is about three times of equivalent petroleum, particularly the combustion product is the only water without environmental pollution, which could make it as a most ideal energy carrier [6,7]. Photocatalytic decomposition of water, the use of inexhaustible solar energy to split water into hydrogen, is an ideal avenue to obtain the clean and renewable hydrogen energy [8–13]. Since it is found that TiO_2 could realize photocatalytic decomposition of water in 1972 [14], a series of various semiconductors [15–17] have been used as efficient photocatalysts in the field of photocatalytic hydrogen evolution. However, most semiconductors have the common disadvantages of weak visible-light absorption and high recombination rate of photogenerated electron-hole pairs, which seriously limits their photocatalytic performance for hydrogen evolution [18].

For dye-sensitized system, it often can convert broad-band long-wavelength light in the visible-light region [19–21] and transfer the excited state electrons into the conduction band of semiconductors to further achieve charge carrier separation effectively [22–24]. Due to the low-toxicity and low-price [25], organic dyes are often used in photosensitization process, among which eosin-Y (EY) is apt to be more common. The cocatalyst often is necessary and very important in dye-sensitized system, which can not only provide active sites for trapping photogenerated electrons from organic dyes to promote charge separation, but also consume the photogenerated electrons with hydrogen atoms in time to release the required hydrogen [26,27]. Nakabayashi *et al.* loaded Pt cocatalyst on TiO_2 as the active center to improve the photocatalytic hydrogen evolution activity, which started the research upsurge on cocatalysts in recent decades [28]. Up till now, noble metal cocatalysts, such as Pt, Pd, Au, Ag, Ru and Rh, have been widely adopted to obtain superior photocatalytic hydrogen evolution performances [29,30]. Unfortunately, the scarcity and high price of noble met-

* Corresponding authors.
E-mail addresses: xyliuctbu@126.com (X. Liu), yzhectbu@163.com (Y. He).

https://doi.org/10.1016/j.cclet.2021.09.047
1001-8417/

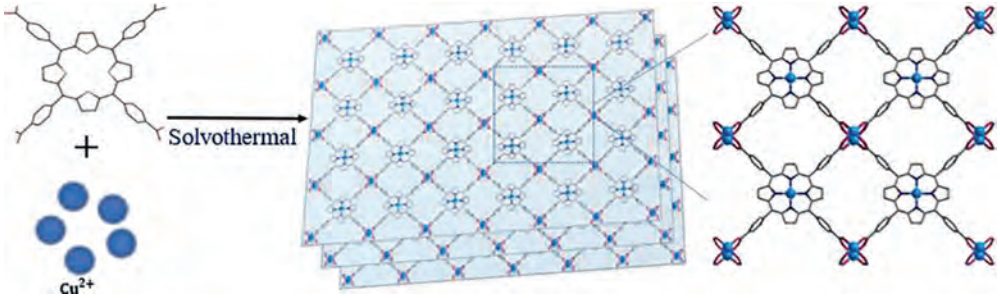

Scheme 1. Synthesis of NS-Cu.

als have greatly restricted their large-scale application in photocatalytic hydrogen evolution fields [31–33]. In addition, although a series of noble-metal-free cocatalysts with low-cost and content-rich also have been studied, the photocatalytic effects are usually not very well relatively, which could be ascribed to the low catalytic efficiency. Therefore, it is very necessary to exploit a cost-effective cocatalyst that could be widely used in large-scale application in photocatalytic hydrogen evolution fields.

Metal-organic frameworks (MOFs), a class of ordered crystal materials assembled by organic linkers and metal nodes, are widely used in photocatalytic fields due to their large specific surface areas and diverse structures [34]. In particular, the metal nodes highly uniformly dispersed in MOFs could be used as independent active sites to participate in photocatalytic reactions, which could greatly improve the atom-utilization efficiency of metal nodes [35]. MOFs-derived phosphides or sulfides often could act as cocatalysts to realize rapid electron transfer for photocatalytic hydrogen evolution, in which the original MOFs usually should be calcinated at high temperature for further modification of the metal nodes accompanied by interminable synthesis steps and inferior atom-utilization efficiency [36,37]. However, the uniformly dispersed metal nodes in original MOFs with very high atom-utilization efficiency as a cocatalyst for photocatalytic hydrogen evolution hardly have been reported.

2D metal-organic frameworks (2D MOFs) have recently emerged as promising catalytic materials [38]. In comparison with bulk MOFs, the metal nodes in 2D MOFs could expose more highly accessible active sites as much as possible to contact with other substrates due to their ultrathin thickness [39,40], thus improving the photocatalytic activity [41]. In this work, several kinds of 2D MOFs were successfully synthesized by solvothermal methods (Scheme 1), in which 5,10,15,20-tetrakis(4-carboxyphenyl porphyrin derivatives as organic ligands and transition-metal molecular cluster as metal nodes. Various experimental technologies especially cyclic voltammetry (CV) and Mott-Schottky (M-S) had been adopted to study the charge-transfer property of photo-generated electron-hole pairs, it was found that the Cu-clusters played a very important role in the electron transfer process, that was, the photo-generated electron transfer from excited state EY to the Cu-clusters for efficient hydrogen evolution. The excellent photocatalytic performance could be attributed to the reversible oxidation–reduction process of Cu^{II}/Cu^{I}, which had excellent electron-receiving and electron-outputting capabilities [42]. To the best of our knowledge, this work represented the first example employing the uniformly dispersed metal nodes of 2D MOFs as a cost-effective noble-metal-free cocatalyst for realizing efficient photocatalytic hydrogen evolution. This strategy might be amenable to developing low price cocatalysts with high atom-utilization efficiency for photocatalytic water splitting.

The synthesis of porphyrin ligand (TCPP) was described in Supporting information.

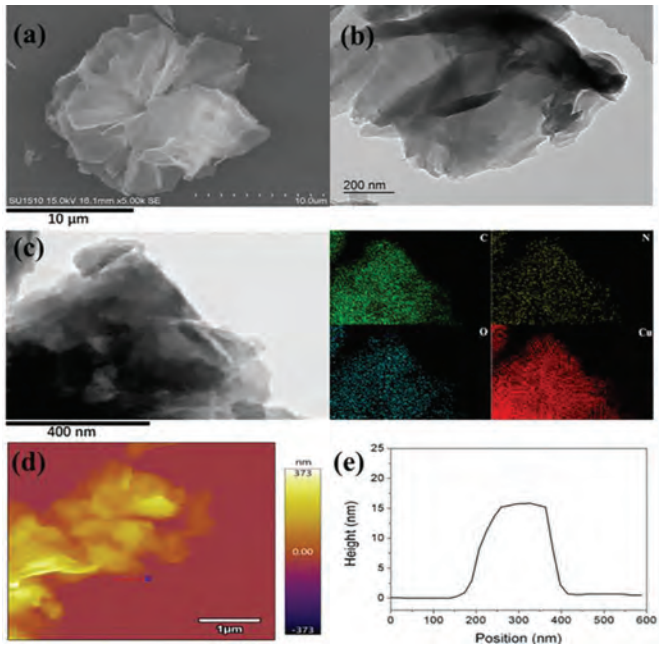

Fig. 1. (a) SEM image, (b) TEM image, and (c) mapping of NS-Cu. (d) AFM image, and (e) corresponding height profile of NS-Cu.

NS-Cu was synthesized by following steps: Add 12 mL of DMF and EtOH (v:v = 3:1) mixture into a 25 mL capped vial, then add 3.6 mg $Cu(NO_3)_2{\cdot}3H_2O$, 10 μL TFA and 10.0 mg PVP. Then TCPP solution (4.0 mg, 3 mL DMF, 1 mL EtOH) was added to the mixture dropwise under stirring. The vials were kept at 80 °C for 4 h, the obtained products were centrifuged and washed with EtOH twice after cooling to room temperature, and finally dried to obtain the product, recorded as NS-Cu.

Synthesis of NS-Zn and NS-Cd: NS-Cd and NS-Zn were prepared by a similar method described in Supporting information.

The crystal structure of NS-Cu was determined by X-ray diffraction (XRD). In Fig. S1 (Supporting information), the NS-Cu had four characteristic diffraction peaks at 7.62°, 9.00°, 12.04° and 19.38° respectively, which could be attributed to (110), (002), (210) and (004) planes [43,44]. Scanning electron microscopy (SEM) image of NS-Cu was shown in Fig. 1a, in which it could be found that the NS-Cu presented a morphology similar to a 2D nanosheet flower with multilayer flakes that was in line with the transmission electron microscopy (TEM) (Fig. 1b). The mapping of NS-Cu was shown in Fig. 1c. Atomic force microscopy (AFM) image (Fig. 1d) further demonstrated that the NS-Cu was nano-sheet structure with a thickness of about 15 nm (Fig. 1e). In addition, the porosity of NS-Cu was examined by N_2 adsorption experiments and the Brunauer–Emmett–Teller (BET) surface area of NS-Cu was 335.75 m^2/g. The pore size distribution data (Fig. S6 in Supporting infor-

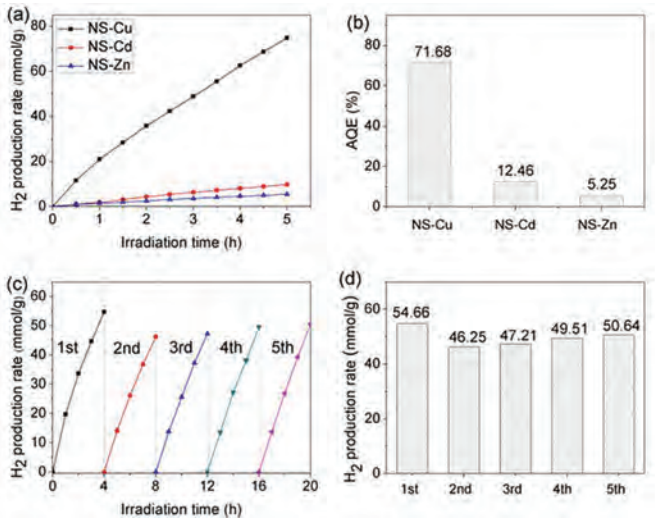

Fig. 2. (a) Photocatalytic hydrogen production ($\lambda \geq 420$ nm) and (b) apparent quantum efficiency (AQE) over NS-M (M = Cu, Cd, Zn), (c) photocatalysis cycle curve and (d) hydrogen production every four hours of NS-Cu.

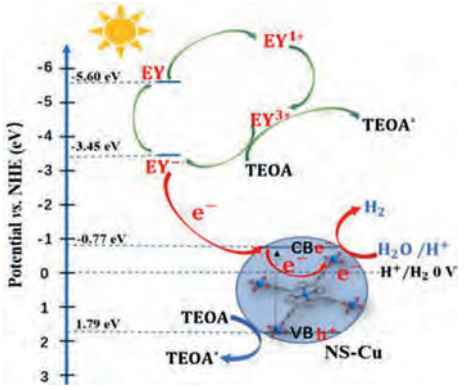

Fig. 3. Possible photocatalytic mechanism diagram of NS-Cu.

mation) showed that NS-Cu had a micropore of 1.20 nm and had other pores with the size of 2.25 nm, which might be caused by the accumulation of NS-Cu during drying [45].

The high-resolution XPS spectrum of C 1s (Fig. S8a in Supporting information) showed three peaks at 284.8 eV, 286.2 eV, 288.4 eV, respectively, which could be assigned to C−C/C=C, C-N and C=O/C=N [46], indicating that the integrity of porphyrin ring was maintained in NS-Cu. In Fig. S8b (Supporting information), there were three peaks of N 1s at 398.7, 399.9 and 400.9 eV, which could be assigned to N=C, N−C and N−H [47]. Fig. S8c (Supporting information) showed two major peaks at 531.8 eV and 533.4 eV, which were attributed to C=O and C−O/O−H. At the same time, it could be found that the peak intensity of C−O/O−H was much weaker than that of C=O [46,47], which proved that the −COOH was successfully coordinated with Cu^{2+} ion. In addition, the spectrum in Fig. S8d (Supporting information) illustrated the oxidation state of the metal node, specifically, the peaks at 935.2 eV and 955.3 eV could be assigned to Cu $2p_{3/2}$ and Cu $2p_{1/2}$ of Cu^{2+}, the weaker peaks at 933.1 eV and 953.0 eV could be assigned to Cu $2p_{3/2}$ and Cu $2p_{1/2}$ of Cu^{+} [46].

As shown in Fig. 2a, the photocatalytic hydrogen evolution performance of all the as-synthesized samples was evaluated under visible-light irradiation. Surprisingly, when the metal nodes were Cu-clusters, the photocatalytic hydrogen evolution rate of the nanosheet NS-Cu could be as high as 15.39 mmol g^{-1} h^{-1}, which was 6 times of NS-Cd and 14 times of NS-Zn. At the same time, the apparent quantum efficiency (AQE) of photocatalytic hydrogen evolution of the three materials was measured, and the results were shown in Fig. 2b. The apparent quantum efficiency of NS-Cu was the highest, which was 71.68%, indicating the highest light utilization. In addition, the photocatalytic hydrogen evolution cycle experiment (Figs. 2c and d) was carried out to detect the photocatalytic stability of the NS-Cu. It could be found that the five cycle test results of NS-Cu were similar, which indicated that the optimal material was relatively stable to a certain extent. The XRD (Fig. S17 in Supporting information) and SEM (Fig. S18 in Supporting information) images of NS-Cu before and after the photocatalytic hydrogen evolution reaction had little difference, which also reflected the good stability of NS-Cu. Furthermore, the hydrogen evolution rate of Cu-clusters nanosheets with different center metals was almost the same (Fig. S9 in Supporting information), which proved that the center metal had almost no effect on the photocatalytic activity.

In addition, the separation and recombination trend of photogenerated electron-hole pairs were also analyzed by photoluminescence spectra (PL) (Fig. S12c in Supporting information). The results showed that the fluorescence intensity of EY solution decreased after adding a certain amount of three kinds of nanosheets. It was worth noting that the fluorescence intensity of (EY + NS-Cu) was the lowest, indicating that the recombination rate of photogenerated electron hole was the lowest, which was consistent with the photocatalytic activity. The fluorescence lifetime of the materials was investigated by transient fluorescence spectrum. As shown in Fig. S13 (Supporting information), NS-Cu had a long fluorescence lifetime, which indicated that it had a long time to maintain the excited state, and the probability of photo generated electrons participating in the photocatalytic reaction was large, so it might have the best photocatalytic activity.

To explore the redox process for hydrogen evolution, the cyclic voltammetry (CV) test was carried out in 0.2 mol/L Na_2SO_4 (pH 7) aqueous solution. In Fig. S12d (Supporting information), NS-Cu had a pair of well-defined redox peaks at −0.05 V and −0.46 V *vs.* Ag/AgCl, which could be attributed to the reversible oxidation–reduction process of Cu^{II}/Cu^{I}, indicating that NS-Cu had a strong ability to capture and export electrons at the same time. In addition, the redox potentials of Cu-clusters nanosheets with different center metals appeared in the same position (Fig. S14 in Supporting information), which indicated that the redox potentials are independent of the center metals and belonged to the role of Cu-clusters. The above results indicated that the electrons were transferred to the Cu-clusters *via* the traditional ligand-to-metal charge transfer (LMCT) pathway, not to the porphyrin center. When the metal nodes were Zn-clusters, its weak current response indicated that the electron transfer activity was relatively poor. In addition, when the metal nodes were Cd-clusters, it could be found that there was a redox potential at −1.11 V, which was more negative than that of NS-Cu. The results indicated that NS-Cd had weaker electron capturing ability than NS-Cu, which was consistent with the hydrogen evolution results.

In Fig. 3, EY absorbed photons to form a single excited state EY^{1*} under visible light irradiation, and then formed a triple excited state EY^{3*} through intersystem crossing (ISC) [48,49]. Finally, EY^{3*} was quenched by TEOA to produce $EY^{\bullet-}$. In this process, NS-Cu could also absorb some photons, making the electrons in VB excited into CB. Because the LUMO level (−3.45 eV) [49] of the excited state EY was more negative than the CB level of NS-Cu, the electrons were transferred from $EY^{\bullet-}$ to the CB level of NS-Cu, and then from the Cu-clusters of NS-Cu to H_2O or H^+ to complete the evolution process of H_2 (E_{H^+/H_2} = 0 V). In addition, the VB poten-

tial of NS-Cu was higher than the redox potential of TEOA (0.84 eV) [50], so the holes also could be used to oxidize TEOA to consume holes to reduce electron-hole recombination [51].

In conclusion, we prepared several 2D porphyrin MOFs nanosheets *via* a simple solvothermal method and studied their photocatalytic hydrogen production performance in dye-sensitized system. It was found that the optimal NS-Cu with a narrow band gap of 2.56 eV had the highest hydrogen production rate of 15.39 mmol g^{-1} h^{-1}. Through further mechanism investigation, it could be seen that the excited photo-generated electron transfer from the LUMO energy levels of EY* to the uniformly dispersed Cu-clusters nodes of NS-Cu for further reduction of H_2O/H^+ to obtain H_2. This work demonstrated that uniformly distributed metal nodes in the original MOFs could be used as economic and effective noble-metal-free cocatalysts with very high atom-utilization efficiency to improve the photocatalytic hydrogen evolution performance in dye-sensitized system.

Declaration of competing interest

No conflicts of interest exit in the submission of this manuscript, and manuscript is approved by all authors for publication.

Acknowledgments

This work was supported by the National Natural Science Foundation of China (Nos. 21502012, 22001026), the Youth Project of Science and Technology Research Program of Chongqing Education Commission of China (Nos. KJQN201900838, KJQN201800836, KJQN201900842), the Chongqing Science and Technology Commission (Nos. cstc2018jcyjAX0531, cstc2017jcyjAX0404, cstc2020jcyj-msxmX0830), Student Science and Technology Innovation Fund Project of Chongqing Technology and Business University (No. 20328).

Supplementary materials

Supplementary material associated with this article can be found, in the online version, at doi:10.1016/j.cclet.2021.09.047.

References

[1] L. Wu, Q. Li, C. Yang, et al., J. Mater. Chem. A 6 (2018) 20947–20955.
[2] Z. Hu, X. Zhang, Q. Yin, et al., Nano Energy 60 (2019) 775–783.
[3] R. Shen, D. Ren, Y. Ding, et al., Sci. China Mater. 63 (2020) 2153–1288.
[4] S. Wageh, A.A. A.l-Ghamdi, R. Jafer, X. Li, P. Zhangc, Chin. J. Catal. 42 (2021) 667–669.
[5] Z. Jiang, Q. Chen, Q. Zheng, et al., Acta Phys. Chim. Sin. 37 (2021) 1–11.
[6] M.P. S.ociety, Chem. Rev. 107 (2007) 3900–3903.
[7] C. Acar, I. Dincer, J. Clean. Prod. 218 (2019) 835–849.
[8] H. Wang, X. Hu, Y. Ma, D. Zhu, T. Li, J. Wang, Chin. J. Catal. 41 (2020) 95–102.
[9] J. Shen, R. Wang, Q. Liu, et al., Chin. J. Catal. 40 (2019) 380–389.
[10] Z. Liang, R. Shen, Y.H. Ng, et al., J. Mater. Sci. Technol. 56 (2020) 89–121.
[11] R. Shen, Y. Ding, S. Li, et al., Chin. J. Catal. 42 (2020) 25–36.
[12] X. Li, Y. Li, H. Wang, et al., ACS Appl. Energy Mater. 4 (2021) 730–736.
[13] R. Shen, X. Lu, Q. Zheng, et al., Sol. RRL. 5 (2021) 2100177.
[14] A. Fujishima, K. Honda, Nat. New Biol. 238 (1972) 37–38.
[15] R. Shen, K. He, A. Zhang, et al., Appl. Catal. B: Environ. 291 (2021) 120104.
[16] G. Shi, X. Zhang, J. Li, et al., Nano Res. 10 (2017) 2377–2385.
[17] X. Li, F. Wu, Y. Jin, et al., Inorg. Chem. Commun. 110 (2019) 107604.
[18] B. Chai, C. Liu, C. Wang, J. Yan, Z. Ren, Chin. J. Catal. 38 (2017) 2067–2075.
[19] Q. Wali, R. Jose, SnO_2 dye-sensitized solar cells, in: S. Thomas, E.H.M. Sakho, N. Kalarikkal, O.S. Oluwafemi, J. Wu (Eds.), Nanomaterials for Solar Cell Applications, Elsevier, 2019, pp. 205–285.
[20] X. Zhang, T. Peng, S. Song, J. Mater. Chem. A 4 (2016) 2365–2402.
[21] Y. Wang, J. Hong, W. Zhang, R. Xu, Catal. Sci. Technol. 3 (2013) 1703–1711.
[22] H. Hagiwara, N. Ono, T. Inoue, H. Matsumoto, T. Ishihara, Angew. Chem. 118 (2006) 1448–1450.
[23] Y.P. Yuan, L.S. Yin, S.W. Cao, et al., Appl. Catal. B: Environ. 168–169 (2015) 572–576.
[24] L. Wang, S. Duan, P. Jin, et al., Appl. Catal. B: Environ. 239 (2018) 599–608.
[25] P. Chowdhury, S. Athapaththu, A. Elkamel, A.K. R.ay, Sep. Purif. Technol. 174 (2017) 109–115.
[26] A. Of, J. Yang, L. Berkeley, C. Physics, C.L. G.uiyang, Acc. Chem. Res. 46 (2013) 1900–1909.
[27] S. Peng, Y. Cao, F. Zhou, Z. Xu, Y. Li, Appl. Surf. Sci. 487 (2019) 315–321.
[28] S. Nakabayashi, A. Fujishima, K. Honda, Chem. Phys. Lett. 102 (1983) 464–465.
[29] T. Takata, J. Jiang, Y. Sakata, et al., Nature 581 (2020) 411–414.
[30] J. Ran, M. Jaroniec, S.Z. Qiao, Adv. Mater. 30 (2018) 1–31.
[31] S. Han, Q. Yun, S. Tu, et al., J. Mater. Chem. A 7 (2019) 24691–24714.
[32] B. Ma, D. Li, X. Wang, K. Lin, ChemSusChem 11 (2018) 3871–3881.
[33] R. Shen, J. Xie, Y. Ding, et al., ACS Sustain. Chem. Eng. 7 (2019) 3243–3250.
[34] H. Zhang, Z. Yu, R. Jiang, et al., Renew. Energy 168 (2021) 1112–1121.
[35] Y.B. H.uang, J. Liang, X.S. W.ang, R. Cao, Chem. Soc. Rev. 46 (2017) 126–157.
[36] Y. Yang, C. Zhou, W. Wang, et al., Chem. Eng. J. 405 (2021) 126547.
[37] J. Ran, J. Zhang, J. Yu, M. Jaroniec, S.Z. Q.iao, Chem. Soc. Rev. 43 (2014) 7787–7812.
[38] Y. Wang, L. Feng, J. Pang, et al., Adv. Sci. 6 (2019) 1802059.
[39] Y. Zhou, L. Zheng, D. Yang, et al., Small Methods 5 (2021) 2000991.
[40] K. Jayaramulu, D.P. D.ubal, A. Schneemann, et al., Adv. Funct. Mater. 29 (2019) 1–11.
[41] Q. Zuo, T. Liu, C. Chen, et al., Angew. Chem. Int. Ed. 58 (2019) 10198–10203.
[42] X. Chen, S. Xiao, H. Wang, et al., Angew. Chem. Int. Ed. 59 (2020) 17182–17186.
[43] M. Zhao, Y. Wang, Q. Ma, et al., Adv. Mater. 27 (2015) 7372–7378.
[44] Q. Lu, M. Zhao, J. Chen, et al., Small (2016) 4669–4674.
[45] E.Y. Choi, C.A. W.ray, C. Hu, W. Choe, CrystEngComm 11 (2009) 553–555.
[46] Y. Li, Z. Gao, F. Chen, et al., ACS Appl. Mater. Interfaces 10 (2018) 30930–30935.
[47] Y. Zhao, J. Wang, R. Pei, J. Am. Chem. Soc. 142 (2020) 10331–10336.
[48] Z. Qin, Y. Chen, Z. Huang, J. Su, L. Guo, J. Mater. Chem. A 5 (2017) 19025–19035.
[49] L. Yang, J. Huang, L. Shi, et al., Nano Energy 36 (2017) 331–340.
[50] J. Xu, Y. Qi, L. Wang, Appl. Catal. B: Environ. 246 (2019) 72–81.
[51] A. Kudo, Y. Miseki, Chem. Soc. Rev. 38 (2009) 253–278.